Journal of Biomechanics 159 (2023) 111803

Contents lists available at ScienceDirect

Journal of Biomechanics

journal homepage: www.elsevier.com/locate/jbiomech

A computational study of fluid transport characteristics in the brain parenchyma of dementia subtypes

Zeyan Li [a,d], Duanduan Chen [a,d], Zhiye Li [c], Haojun Fan [a], Liwei Guo [b,*], Binbin Sui [c,*], Yiannis Ventikos [b,d,1]

[a] Wenzhou Safety (Emergency) Institute, Tianjin University, Wenzhou, China
[b] Department of Mechanical Engineering, University College London, London, United Kingdom
[c] Tiantan Neuroimaging Center for Excellence, China National Clinical Research Center for Neurological Diseases, Beijing Tiantan Hospital, Beijing, China
[d] School of Life Science, Beijing Institute of Technology, Beijing, China

ARTICLE INFO

Keywords:
Alzheimer's disease
Vascular dementia
Poroelasticity
CSF
Blood perfusion

ABSTRACT

The cerebral environment is a complex system consisting of parenchymal tissue and multiple fluids. Dementia is a common class of neurodegenerative diseases, caused by structural damages and functional deficits in the cerebral environment. In order to better understand the pathology of dementia from a cerebral fluid transport angle and provide clearer evidence that could help differentiate between dementia subtypes, such as Alzheimer's disease and vascular dementia, we conducted fluid–structure interaction modelling of the brain using a multiple-network poroelasticity model, which considers both neuropathological and cerebrovascular factors. The parenchyma was further subdivided and labelled into parcellations to obtain more localised and detailed data. The numerical results were converted to computed functional images by an in-house workflow. Different cerebral blood flow (CBF) and cerebrospinal fluid (CSF) clearance abnormalities were identified in the modelling results, when comparing Alzheimer's disease and vascular dementia. This paper presents our preliminary results as a proof of concept for a novel clinical diagnostic tool, and paves the way for a larger clinical study.

1. Introduction

Alzheimer's disease (AD) and vascular dementia (VaD) are two common subtypes of dementia (Di Marco et al., 2014; Dsm et al., 2000). AD is mainly characterised by the accumulation of toxic extracellular beta-amyloid (Aβ) and hyperphosphorylated *tau* (Bateman et al., 2012; Jack et al., 2013; Lorenzo et al., 2000), whereas the pathology of VaD suggests impaired cerebral vasculature/perfusion (Braun and Iliff, 2020; Kapasi and Schneider, 2016). Recent research has proposed a cerebrovascular hypothesis for AD as well (Canobbio et al., 2015; Janota et al., 2016; Vardakis et al., 2019), which implied that hemodynamic disturbances and neurodegeneration acted in a coupled manner (Ashby et al., 2012; Liu et al., 2018; Sabayan et al., 2012; Torre, 2004). Thus, there may be coupling of impaired cerebral blood flow (CBF) and reduced cerebrospinal fluid (CSF) clearance (Iliff et al., 2012; Lee et al., 2020; Simon and Iliff, 2016; Zhang et al., 2012). Meanwhile, previously pure VaD was believed to only refer to infarction and white matter lesions (Goujon et al., 2018; Kalaria, 2002). However, more recent publications have identified that some cortical functions of VaD patients gradually deteriorate over time due to neurovascular coupling (Donahue et al., 2017; Kim et al., 2020; Lecrux et al., 2019; Marina et al., 2020). These overlapping clinical characteristics make the differentiation between AD and VaD not always accurate.

It is difficult to obtain dementia biomarkers directly measured *in vivo* (Bateman et al., 2006). Neuroimaging techniques play an important role in the diagnosis of dementia (Bateman et al., 2006; Clark et al., 2017; Yan et al., 2018; Zhang et al., 2017). Although amyloid markers can be acquired early to diagnose AD, sensitive and reliable clinical biomarkers are still lacking (Jiang et al., 2017). In this respect, numerical modelling can provide novel tools to help understand mixed pathology, identify targets for intervention, and determine the interaction between VaD and AD pathologies. In this paper, we present the preliminary results of integrating a fluid–structure interaction model – the multiple-network poroelastic theory (MPET) (Guo et al., 2020; Tully and Ventikos, 2011; Vardakis et al., 2013), into a computational modelling platform to investigate dementia subtypes. This computational model has been

* Corresponding authors.
E-mail addresses: liwei.guo@ucl.ac.uk (L. Guo), reneesui@163.com (B. Sui).
[1] Present address: Faculty of Engineering, Monash University, Clayton, Victoria, Australia.

https://doi.org/10.1016/j.jbiomech.2023.111803
Accepted 15 September 2023
Available online 16 September 2023

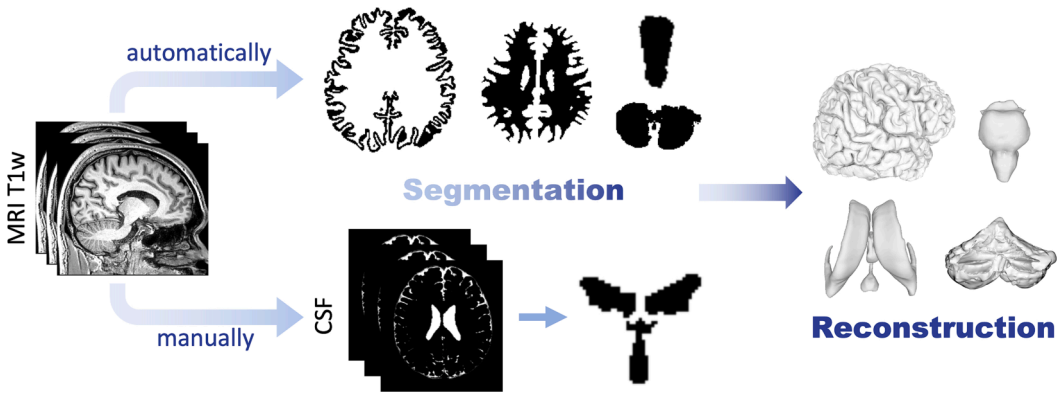

Fig. 1. The workflow of creating the brain model.

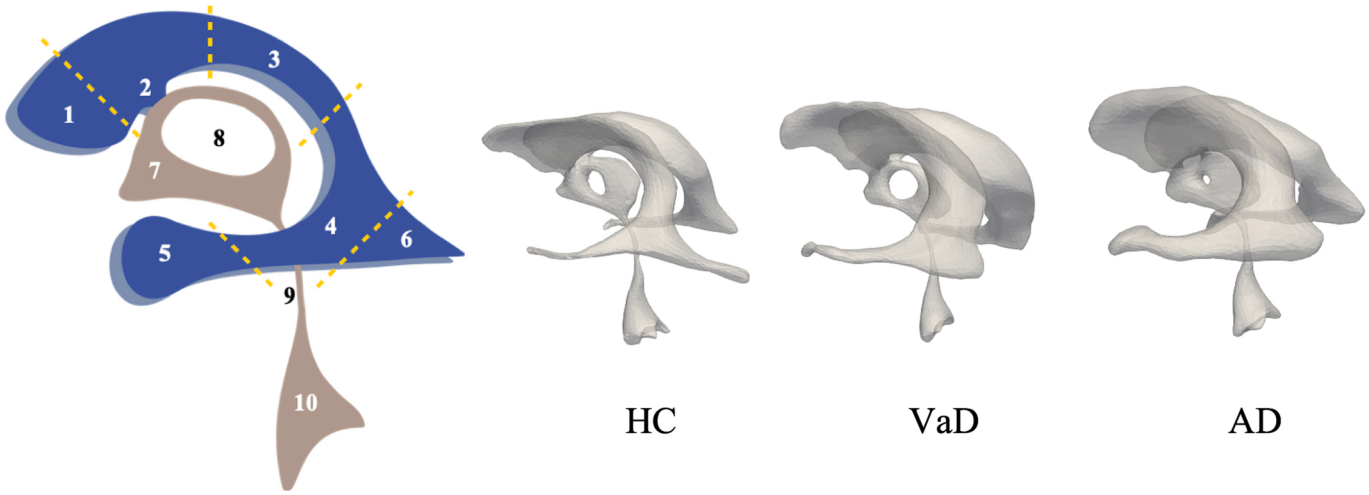

Fig. 2. The ventricular system in the reconstructed brain models of the three subjects. (1) FH, frontal horn; (2) MF, Monro foramen; (3) VB, ventricular body; (4) VT, ventricular trigone; (5) TH, temporal horn / IH, inferior horn; (6) OH, occipital horn / PH, posterior horn; (7) THV, third ventricle; (8) IA, interthalamic adhesion; (9) CA, cerebral aqueduct; (10) FV, fourth ventricle.

validated in a previous study of stroke (Guo et al., 2019).

2. Methodology

2.1. Subject recruitment and data collection

Two patients admitted to Beijing Tiantan Hospital (Beijing, China), presenting with onset of VaD or AD were randomly brought into this study. The diagnosis of the AD patient (female, 62 years old) was confirmed by an amyloid-PET (Positron Emission Tomography) scan and the VaD patient (female, 69 years old) had an ischemic stroke before onset of dementia. A healthy control (HC) subject without dementia (female, 72 years old) was also recruited to provide baseline data for comparison. All of the subjects gave informed consent, and the study was approved by the Institutional Review Board of Beijing Tiantan Hospital Affiliated to Capital Medical University in China. The detailed parameters for data collection can be found in the Supplementary Material.

2.2. MRI post-processing

Segmentation and reconstruction of the brain model were performed following the workflow shown in Fig. 1. Freesurfer (Fischl et al., 2004) was used to automatically segment the brain geometries from T1w images. The ventricular geometries (Fig. 2) are highly subject-specific in patients with neurovascular abnormalities; for example, clear atrophy can be seen in the AD patient – the brain parenchyma volumes of the VaD and AD patients are 945.54 ml and 942.82 ml, respectively, compared with 1149.92 ml of the healthy control. Thus, we further performed manual segmentation based on CSF images using an embedded T1 segmentation module in the SPM12 toolbox (Penny et al., 2007). We then discretised the brain model into a computational mesh using ANSYS (ANSYS, Inc., Canonsburg, USA). The mesh resolution used has been shown to satisfy strict grid convergence criteria (Guo et al., 2018).

We further divided the brain into ten regions (Fig. 3) to obtain region-specific results in post-processing. Due to the different mechanical responses between the white matter (WM) and the grey matter (GM), we calculated fractional anisotropy (FA) values from DTI (Diffusion Tensor Imaging) images using a standard FSL (the FMRIB Software Library) routine, and then mapped the FA values to each tetrahedral element as an index to determine whether the element belongs to WM or GM (Li et al., 2022). More specifically, we calculated the centroid of each tetrahedral element in the mesh space and assigned the FA value from the voxel that contains this centroid. The DTI-based optimisation worked better in the simulations compared with reconstruction purely using structural description based on T1w images.

2.3. MPET model and computed functional images

The complete description of the multiple-network poroelastic theory (MPET) was given in previous publications (Guo et al., 2020; Tully and

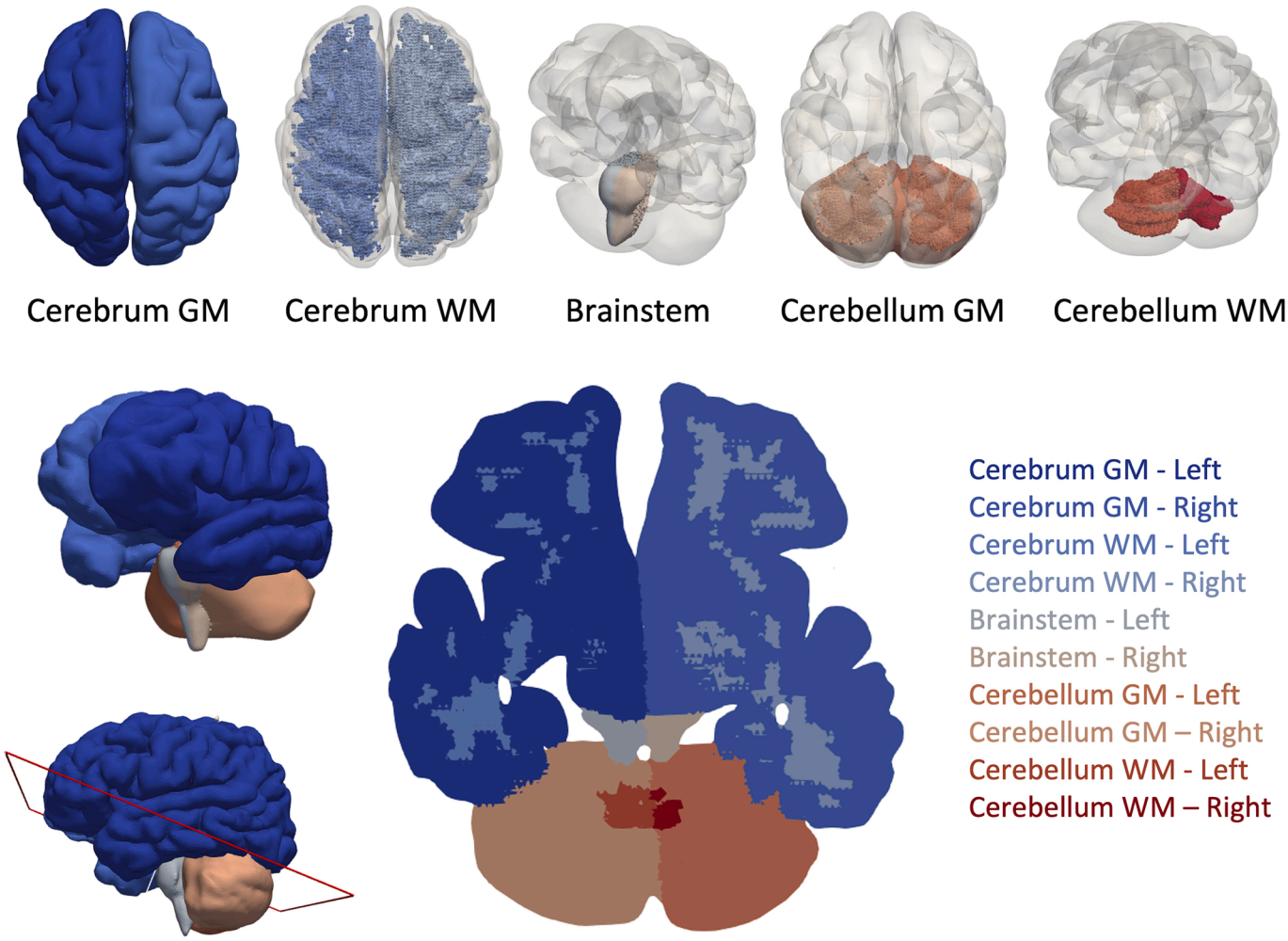

Fig. 3. Ten regional labels in the computational domain.

Table 1
Global means of CBF and CSF clearance rate from MPET simulations.

Subject	mean CBF (ml/100 g/min)	mean CSF clearance rate (10^{-6} m/s)
VaD	23.497	2.178
AD	12.160	2.318
HC	21.575	2.549

Ventikos, 2009; Tully and Ventikos, 2011). By coupling Darcy flow and elastic deformation, the MPET model assumes the brain as porous tissue perfused by four "types" of fluids – the arterial blood, the arteriole/capillary blood, the venous blood and the CSF/ISF. Filtration velocities (represented by Darcy velocities) of the arteriole/capillary and the CSF/ISF compartments are assumed to represent cerebral blood perfusion and CSF clearance, respectively, which are the main variables investigated in this paper. Due to the lack of patient-specific data, we used previous data (Guo et al., 2019) for the arterial compartment; the other boundary conditions and parameters are mainly derived from literature (details given in Guo et al., 2020). This MPET formulation is cast in an in-house 3D transient finite element model.

Furthermore, we developed an in-house MATLAB script to process the numerical results to obtain regional data for each anatomical parcellation. In the data projection, the values of variables of interest in each voxel are calculated as the average of the nodal values in the tetrahedral mesh within this voxel. Therefore, the numerical results can be visualised as standard images, which are called MPET-Perfusion and MPET-Clearance modalities. Then, the computed functional images are registered to a standard brain template, such as AAL 3 (automated anatomical labelling atlas 3, *https://www.oxcns.org/aal3.html*) (Rolls et al., 2020).

2.4. Workflow to identify potential abnormal parcellations

In order to quantify the hydromechanical differences between the VaD and AD patients, we further processed the CBF and CSF clearance rate data following the steps listed below, to identify potential abnormal parcellations (Fig. 1 in the Supplementary Material):

1. Calculate the differences (including the regional mean D_i and the global mean D_{mean}) of the two variables of interest – CBF and CSF clearance rate, between HC and VaD/AD subjects, respectively.
2. Compare the absolute value of each regional difference with the absolute value of the global mean difference and label the parcellations where the magnitude of the regional difference is greater than the global mean difference as potential abnormal parcellations (dataset a for CBF and dataset c for CSF clearance rate).
3. Determine whether the regional difference shows the same sign as the global mean difference and label the parcellations with opposite signs (dataset b for CBF and dataset d for CSF clearance rate).
4. Find symmetrically distributed (both in the left and right hemispheres) parcellations to create sub-datasets a_s, b_s, c_s, d_s, and calculate the intersection of sub-datasets a_s and c_s. The majority of previous studies mainly focused on lesions induced by unilateral

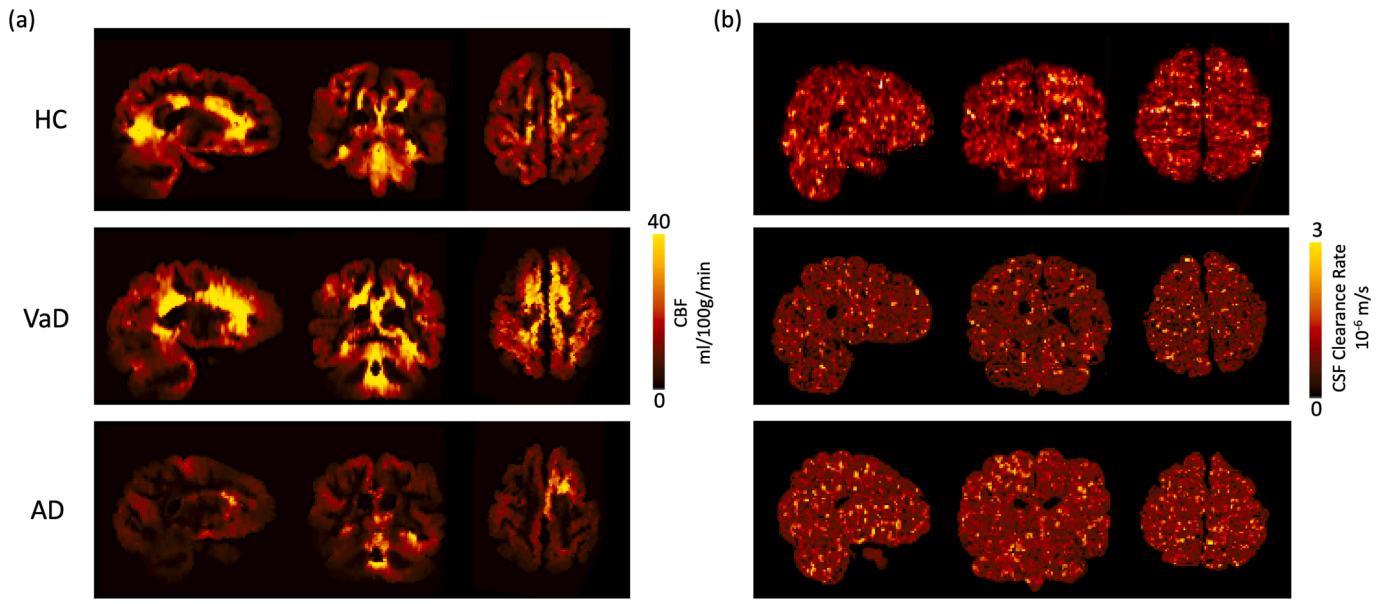

Fig. 4. Voxel-based MPET-Perfusion (a) and MPET-Clearance (b) images of the healthy control, VaD and AD patients.

vascular pathology (Ding et al., 2016; Mitelpunkt et al., 2020; Van et al., 2018). Here we expand our focus to find parcellations that are abnormal both in the left and right hemispheres.

3. Results

3.1. Global flow dynamics

The numerical results show normal values of global CSF pressure, which represents intracranial pressure, in all of the three subjects. However, abnormalities were found in the global mean values of CBF and CSF clearance rate in the VaD and AD patients (Table 1); both show reduced CSF clearance rate compared with that of the healthy control (Ray et al., 2019). Moreover, although the VaD patient shows similar CBF level as the healthy control (Fahlstrm et al., 2021; Henriksen et al., 2012; Lassen, 1985; Rostrup et al., 2005; Zhang et al., 2014), the AD patient shows a substantial decline.

3.2. Regional flow dynamics

Previous research showed high frequency of small cortical or subcortical lesions in specific brain structures of dementia patients (Fyfe, 2017; Knopman et al., 2021; Mitelpunkt et al., 2020; Sabayan et al., 2012). Therefore, we mapped MPET modelling results back to the voxel space and generated MPET-Perfusion and MPET-Clearance images to compare the regional data (Fig. 4).

The complete data of all the 166 parcellations can be found in Table 1 of the Supplementary Material. The potential abnormal parcellations in the VaD and AD patients are shown in Fig. 5, which were identified by applying the workflow listed in Section 2.4 and include the ones with marked differences in magnitude (datasets *a* and *c*) and opposite trends (datasets *b* and *d*). The complete data can be found in Table 2 of the Supplementary Material. We then further identified parcellations with symmetrical abnormalities in both the left and right hemispheres as sub-datasets a_s and c_s (Fig. 6), and the intersection $a_s \cap c_s$ is regarded as disease-associated regions – 34 and 27 such regions were found in VaD and AD patients, respectively (Table 2, also highlighted by yellow in Table 3 of the Supplementary Material).

4. Discussion

It can be seen from Table 2 that the cerebrum has the most different distributions of disease-associated regions between the VaD and AD patients. Fluid dynamics abnormalities (intersection of datasets $a_s \cap c_s$) are concentrated in the parietal lobe of the VaD patient, but they mainly occur in the frontal lobe of the AD patient. Moreover, the basal ganglia is also a characteristic region in VaD pathology. VaD patients normally show motor retardation and response delay, which are related to the functional integrity of the sensory cortex and motor cortex; the areas where abnormal fluid dynamics are observed in the VaD patient (e.g. the superior parietal gyrus, inferior parietal gyrus, caudate nucleus and putamen) coincide with the parietal lobe and the basal ganglia. Although both the VaD and AD patients show abnormalities in the limbic system, only the AD patient shows differences in para-hippocampus and temporal pole. These characteristics may imply brain parenchymal lesions in the adjacent regions, such as the hippocampus and temporal lobe, during the onset of AD (Livingston et al., 2020), which coincide with areas where disease biomarkers (e.g. atrophy) are observed. This is also consistent with other work, which found significantly lower CBF values in the AD group in most frontal and temporal lobes when comparing with VaD patients (Zimny et al., 2007), and the temporal lobes are the most severely affected regions (Buffington et al., 2013; Roman and Pascual, 2012; Zimny et al., 2007). Abnormal parcellations in the cerebellum, thalamus and brainstem look less different between the VaD and AD patients than in the cerebrum, which may mean disturbances spread from the cerebrum of both VaD and AD patients into the cerebellum, thalamus and brainstem (Kapasi and Schneider, 2016).

Vascular lesions in the WM are also important in VaD and also contribute to AD. However, the standard template AAL3 does not provide detailed WM parcellations. Therefore, we calculated the CBF and CSF clearance rate in the entire WM of the cerebrum and cerebellum, respectively (Table 3). Three main findings can be summarised here. Firstly, the mean CBF in WM distribute asymmetrically between the left and right cerebral hemispheres in both VaD and AD patients. In addition, all of the WM regions of the AD patient show reduced blood flow. Secondly, CSF clearance rates are relatively low in both VaD and AD patients except the cerebrum of the AD patient. Thirdly, the lowest CSF clearance rate in Table 3 appears to be in the left cerebral hemisphere of the VaD patient, whereas the CBF is the highest, which may mean that

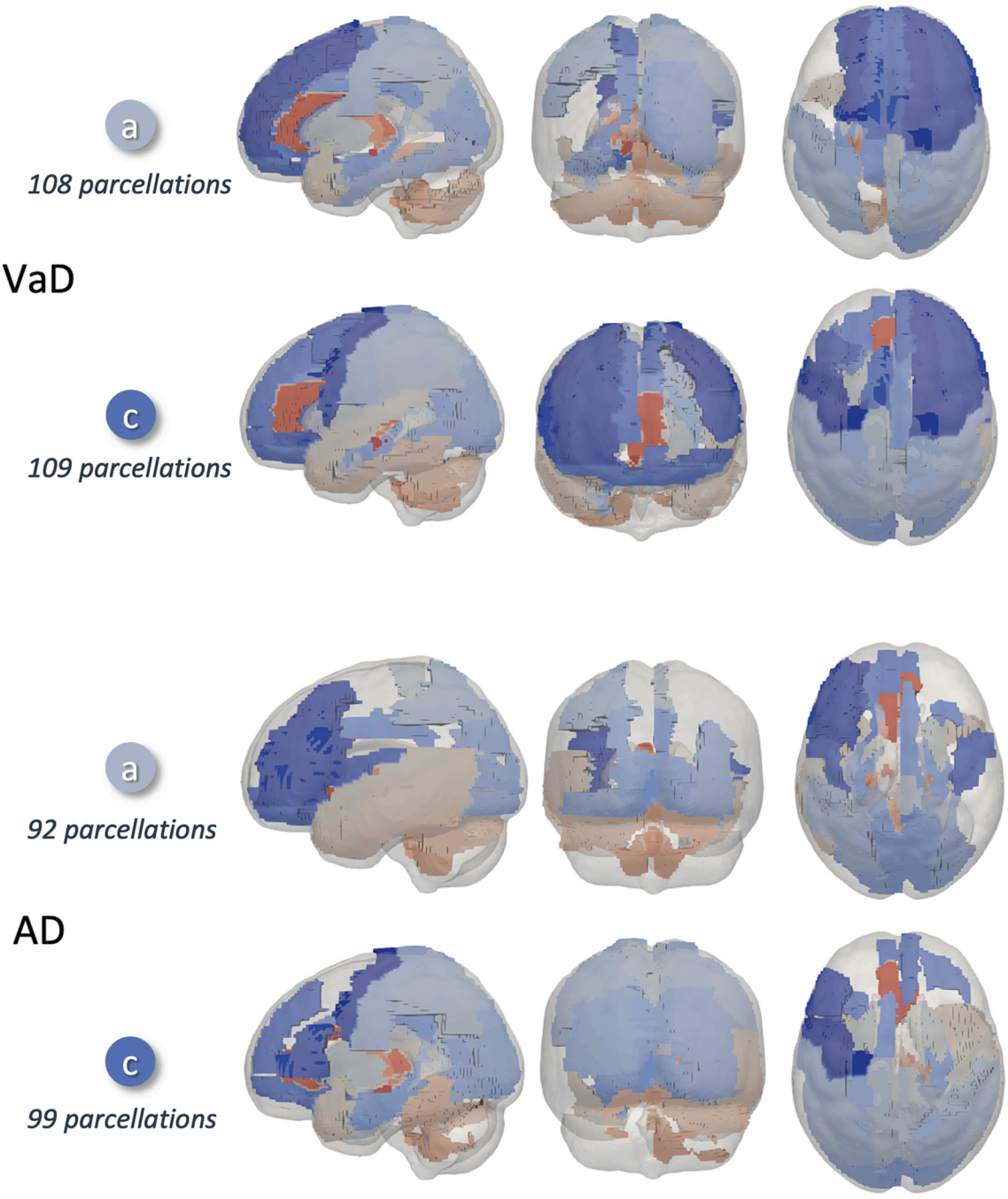

Fig. 5. Visualisation of potential abnormal parcellations (datasets *a* and *c*) in the VaD and AD patients viewed in three orthogonal directions, respectively. Regarding the VaD patient, 108 out of the 166 parcellations were found as regions with abnormal CBF (dataset *a*) and 109 parcellations with abnormal CSF clearance rate (dataset *c*). For the AD patient, CBF abnormalities were found in 92 parcellations (dataset *a*) and abnormal CSF clearance rates in 99 parcellations (dataset *c*).

the vascular damage causes fluid transport impairment in the downstream to the CSF.

The computed functional images (MPET-Perfusion and MPET-Clearance) created by the new workflow can be processed as any standard imaging modality, which makes it more convenient and versatile for the wider community. However, the major limitation of the current work is the small sample size, which only includes one patient of each disease and one healthy control. Another limitation is the results are more qualitative than quantitative, which mainly suggest relative comparison rather than specific data ranges to differentiate between dementia subtypes. These preliminary findings should be further investigated by larger datasets.

5. Conclusions

This paper investigated blood perfusion and CSF clearance rate of dementia subtypes by computational modelling. Our preliminary results show abnormalities in the temporal lobes and adjacent regions of Alzheimer's disease and the frontal lobes of pure vascular dementia, respectively. This paper presents the proof of concept for a novel clinical diagnostic tool.

CRediT authorship contribution statement

Zeyan Li: Conceptualization, Formal analysis, Investigation,

Table 2
Parcellations identified as disease-associated regions.

	VaD	AD
Cerebrum	parietal lobe (postcentral gyrus, superior parietal gyrus and inferior parietal gyrus), the limbic system (cingulum gyrus and amygdala) and basal ganglia (caudate nucleus and putamen)	frontal lobe (olfactory cortex), the limbic system (temporal pole, anterior cingulate subgenual cortex, parahippocampal gyrus and amygdala)
Cerebellum	lobe (semilunar lobule) and vermis (lingula and central lobule)	lobe (flocculus) and vermis (lingula, central lobule and nodule)
Thalamus	lateral posterior and geniculate	reuniens
Brainstem	locus coeruleus and raphe nucleus	substantia nigra pars compacta, red nucleus, locus coeruleus and raphe nucleus

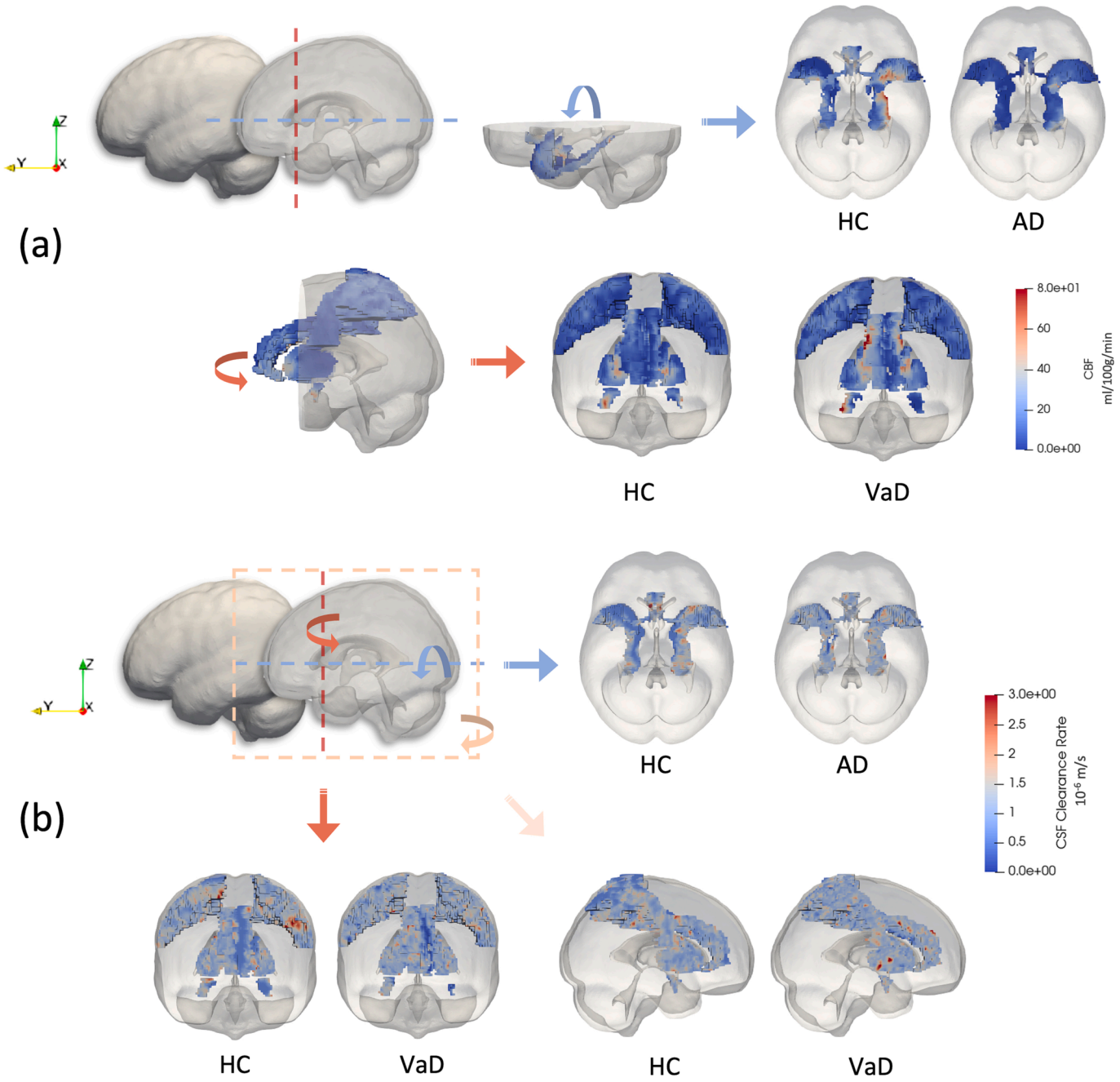

Fig. 6. (a) Parcellations with symmetrical abnormal CBF (dataset a_s) in the cerebrums of the VaD and AD patients. Almost all of the regions show low perfusion in the AD patient, whereas the VaD patient only exhibits local high or low perfusion within the parcellations. (b) Parcellations with symmetrical abnormal CSF clearance rate (dataset c_s) in the cerebrums of the VaD and AD patients. Similar to the CBF results, the VaD patient shows local lesions with very high clearance rate.

Table 3
Means of CBF and CSF clearance rate in WM.

Subject	mean CBF (ml/100 g/min)				mean CSF clearance rate (10^{-6} m/s)			
	Cerebrum		Cerebellum		Cerebrum		Cerebellum	
	L	R	L	R	L	R	L	R
VaD	19.015	15.000	9.672	8.384	1.767	1.878	2.438	2.292
AD	9.763	6.590	6.691	5.328	2.803	2.457	2.227	2.136
HC	15.350	14.322	10.523	8.924	2.268	2.175	3.219	2.997

Methodology, Software, Writing - original draft, Writing - review & editing. **Duanduan Chen:** Conceptualization, Funding acquisition, Resources, Supervision, Writing - review & editing. **Zhiye Li:** Data curation, Investigation, Writing - review & editing. **Haojun Fan:** Formal analysis, Writing - review & editing. **Liwei Guo** Conceptualization, Writing – original draft, Writing – review & editing, Methodology, Supervision, Software. **Binbin Sui:** Conceptualization, Funding acquisition, Resources, Supervision, Writing - review & editing. **Yiannis Ventikos:** Conceptualization, Supervision, Writing - review & editing.

Declaration of Competing Interest

The authors declare that they have no known competing financial interests or personal relationships that could have appeared to influence the work reported in this paper.

Acknowledgements

This study was supported by the Beijing Natural Science Foundation (Z190014), the National Natural Science Foundation of China (62271061) and the Scientific Research Translational Foundation of Wenzhou Safety (Emergency) Institute of Tianjin University.

Appendix A. Supplementary data

Supplementary data to this article can be found online at https://doi.org/10.1016/j.jbiomech.2023.111803.

References

Ashby, E.L., Love, S., Kehoe, P.G., 2012. Assessment of activation of the plasma kallikrein-kinin system in frontal and temporal cortex in alzheimer's disease and vascular dementia. Neurobiol. Aging 33, 1345–1355.
Bateman, G.A., Levi, C.R., Schofield, P., Wang, Y., Lovett, E.C., 2006. Quantitative measurement of cerebral haemodynamics in early vascular dementia and alzheimer's disease. J. Clin. Neurosci. 13, 563–568.
Bateman, R.J., Xiong, C., Benzinger, T., Fagan, A.M., Goate, A., Fox, N.C., Marcus, D.S., Cairns, N.J., Xie, X., Blazey, T.M., 2012. Clinical and biomarker changes in dominantly inherited alzheimer's disease. N. Engl. J. Med. 367, 795–804.
Braun, M., Iliff, J.J., 2020. The impact of neurovascular, blood-brain barrier, and glymphatic dysfunction in neurodegenerative and metabolic diseases. Int. Rev. Neurobiol. 154, 413–436.
Buffington, A.L., Lipski, D.M., Westfall, E., 2013. Dementia: an evidence-based review of common presentations and family-based interventions. J. Am. Osteopath. Assoc. 113, 768–775.
Clark, L.R., Berman, S.E., Rivera-Rivera, L.A., Hoscheidt, S.M., Darst, B.F., Engelman, C. D., Rowley, H.A., Carlsson, C.M., Asthana, S., Turski, P., Wieben, O., Johnson, S.C., 2017. Macrovascular and microvascular cerebral blood flow in adults at risk for alzheimer's disease. Alzheimers Dement (Amst) 7, 48–55.
Di Marco, L.Y., Marzo, A., Munoz-Ruiz, M., Ikram, M.A., Kivipelto, M., Ruefenacht, D., Venneri, A., Soininen, H., Wanke, I., Ventikos, Y.A., Frangi, A.F., 2014. Modifiable lifestyle factors in dementia: a systematic review of longitudinal observational cohort studies. J. Alzheimers Dis. 42, 119–135.
Ding, J., Chen, K., Chen, Y., Fang, Y., Yang, Q., Lv, Y., Lin, N., Bi, Y., Guo, Q., Han, Z., 2016. the left fusiform gyrus is a critical region contributing to the core behavioral profile of semantic dementia. Front. Hum. Neurosci. 10.
Donahue, M.J., Juttukonda, M.R., Watchmaker, J.M., 2017. Noise concerns and post-processing procedures in cerebral blood flow (CBF) and cerebral blood volume (CBV) functional magnetic resonance imaging. Neuroimage 154, 43–58.
Dsm, A.P.A., Association, A., Association, A.P., American Diabetes, A., American, P.A., Association, P., Force, D.S.M.T., Force, T., 2000. Diagnostic and statistical manual of mental disorders. Psychiatry Res. 25, 1–4.
Fahlstrm, M., Appel, L., Kumlien, E., Danfors, T., Lubberink, M., 2021. Evaluation of arterial spin labeling MRI-Comparison with 15O-Water PET on an integrated PET/MR scanner. Diagnostics 11.
Fischl, B., van der Kouwe, A., Destrieux, C., Halgren, E., Segonne, F., Salat, D.H., Busa, E., Seidman, L.J., Goldstein, J., Kennedy, D., Caviness, V., Makris, N., Rosen, B., Dale, A. M., 2004. Automatically parcellating the human cerebral cortex. Cereb. Cortex 14, 11–22.
Fyfe, I., 2017. dementia: Imaging signatures identified for dementia subtypes. Nat. Rev. Neurol. 13, 384–385.
Goujon, A., Mejdoubi, M., Purcell, Y., Banydeen, R., Colombani, S., Arrigo, A., 2018. Can MRI water apparent diffusion coefficient (ADC) value discriminate between idiopathic normal pressure hydrocephalus, alzheimer's disease and subcortical vascular dementia? J. Neuroradiol. 45, 15–22.
Guo, L., Vardakis, J.C., Lassila, T., Mitolo, M., Ravikumar, N., Chou, D., Lange, M., Sarrami-Foroushani, A., Tully, B.J., Taylor, Z.A., Varma, S., Venneri, A., Frangi, A.F., Ventikos, Y., 2018. Subject-specific multi-poroelastic model for exploring the risk factors associated with the early stages of alzheimer's disease. Interface Focus 8, 20170019.
Guo, L., Li, Z., Lyu, J., Mei, Y., Ventikos, Y., 2019. On the validation of a Multiple-Network poroelastic model using arterial spin labeling MRI data. Front. Comput. Neuroence 13.
Guo, L., Vardakis, J.C., Chou, D., Ventikos, Y., 2020. A multiple-network poroelastic model for biological systems and application to subject-specific modelling of cerebral fluid transport. Int. J. Eng. Sci. 147.
Henriksen, O.M., Larsson, H., Hansen, A.E., Grüner, J., Law, I., Rostrup, E., 2012. Estimation of intersubject variability of cerebral blood flow measurements using MRI and positron emission tomography. J. Magn. Reson. Imaging 35, 1290–1299.
Ilaria, C., Aisha, A., Abubaker, C., Visconte, M., Torti, G., 2015. Role of amyloid peptides in vascular dysfunction and platelet dysregulation in alzheimer€s disease. Front. Cell. Neurosci. 9.
Iliff, J.J., Wang, M., Liao, Y., Plogg, B.A., Peng, W., Gundersen, G.A., Benveniste, H., Vates, G.E., Deane, R., Goldman, S.A., 2012. A paravascular pathway facilitates CSF flow through the brain parenchyma and the clearance of interstitial solutes, including amyloid β. Sci. Transl. Med. 4, 147ra111.
Jack, C.R., Knopman, D.S., Jagust, W.J., Petersen, R.C., Weiner, M.W., Aisen, P.S., Shaw, L.M., Vemuri, P., Wiste, H.J., Weigand, S.D., 2013. Tracking pathophysiological processes in alzheimer's disease: an updated hypothetical model of dynamic biomarkers. Lancet Neurol. 12, 207–216.
Janota, C., Lemere, C.A., Brito, M.A., 2016. Dissecting the contribution of vascular alterations and aging to alzheimer's disease. Mol. Neurobiol. 53, 3793–3811.
Jiang, S., Yan, C., Qiao, Z., Yao, H., Jiang, S., Qiu, X., Yang, X., Fang, D., Yang, Y., Zhang, L., Wang, L., Zhang, L., 2017. Mismatch negativity as a potential neurobiological marker of early-stage alzheimer disease and vascular dementia. Neurosci. Lett. 647, 26–31.
Kalaria, R., 2002. Similarities between alzheimer's disease and vascular dementia. J. Neurol. Sci. 203, 29–34.
Kapasi, A., Schneider, J.A., 2016. Vascular contributions to cognitive impairment, clinical alzheimer's disease, and dementia in older persons. Biochim. Biophys. Acta 1862, 878–886.
Kim, C.M., Alvarado, R.L., Stephens, K., Wey, H.Y., Wang, D.J.J., Leritz, E.C., Salat, D.H., 2020. Associations between cerebral blood flow and structural and functional brain imaging measures in individuals with neuropsychologically defined mild cognitive impairment. Neurobiol. Aging 86, 64–74.
Knopman, D.S., Amieva, H., Petersen, R.C., Chetelat, G., Holtzman, D.M., Hyman, B.T., Nixon, R.A., Jones, D.T., 2021. Alzheimer disease. Nat. Rev. Dis. Primers 7, 33.
Lassen, N.A., 1985. Normal average value of cerebral blood flow in younger adults is 50 ml/100 g/min. J. Cereb. Blood Flow Metab. 5, 347–349.
Lecrux, C., Bourourou, M., Hamel, E., 2019. How reliable is cerebral blood flow to map changes in neuronal activity? Auton. Neurosci. 217, 71–79.
Lee, D.S., Suh, M., Sarker, A., Choi, Y., 2020. Brain glymphatic/Lymphatic imaging by MRI and PET. Nucl. Med. Mol. Imaging 54, 207–223.
Li, Z., Chen, D., Guo, L., 2022. Cerebral Perfusion of Multiple-Network Poroelastic Model by Integrating Fractional Anisotropy, AIAM2021: 2021 3rd International Conference on Artificial Intelligence and Advanced Manufacture.
Liu, Y., Braidy, N., Poljak, A., Chan, D.K.Y., Sachdev, P., 2018. Cerebral small vessel disease and the risk of alzheimer's disease: A systematic review. Ageing Res. Rev. 47, 41–48.
Livingston, G., Huntley, J., Sommerlad, A., Ames, D., Ballard, C., Banerjee, S., Brayne, C., Burns, A., Cohen-Mansfield, J., Cooper, C., Costafreda, S.G., Dias, A., Fox, N., Gitlin, L.N., Howard, R., Kales, H.C., Kivimäki, M., Larson, E.B., Ogunniyi, A., Orgeta, V., Ritchie, K., Rockwood, K., Sampson, E.L., Samus, Q., Schneider, L.S., Selbæk, G., Teri, L., Mukadam, N., 2020. Dementia prevention, intervention, and care: 2020 report of the lancet commission. Lancet 396, 413–446.

Lorenzo, A., Yuan, M., Zhang, Z., Paganetti, P.A., Sturchler-Pierrat, C., Staufenbiel, M., Mautino, J., Vigo, F.S., Sommer, B., Yankner, B.A., 2000 May. Amyloid β interacts with the amyloid precursor protein: a potential toxic mechanism in Alzheimer's disease. Nature neuroscience. 3 (5), 460–464.

Marina, N., Christie, I.N., Korsak, A., Doronin, M., Brazhe, A., Hosford, P.S., Wells, J.A., Sheikhbahaei, S., Humoud, I., Paton, J.F.R., Lythgoe, M.F., Semyanov, A., Kasparov, S., Gourine, A.V., 2020. Astrocytes monitor cerebral perfusion and control systemic circulation to maintain brain blood flow. Nat. Commun. 11, 131.

Mitelpunkt, A., Galili, T., Kozlovski, T., Bregman, N., Shachar, N., Markus-Kalish, M., Benjamini, Y., 2020. Novel alzheimer's disease subtypes identified using a data and knowledge driven strategy. Sci. Rep. 10, 1327.

Penny, W.D., Friston, K.J., Ashburner, J.T., Kiebel, S.J., Nichols, T.E.J.N., 2007. Statistical Parametric Mapping: The Analysis of Functional Brain Images.

Ray, L., Iliff, J.J., Heys, J.J., 2019. Analysis of convective and diffusive transport in the brain interstitium.

Rolls, E.T., Huang, C.C., Lin, C.P., Feng, J., Joliot, M., 2020. Automated anatomical labelling atlas 3. Neuroimage 206, 116189.

Roman, G., Pascual, B., 2012. Contribution of neuroimaging to the diagnosis of alzheimer's disease and vascular dementia. Arch. Med. Res. 43, 671–676.

Rostrup, E., Knudsen, G.M., Law, I., Holm, S.R., Larsson, H., Paulson, O.B., 2005. The relationship between cerebral blood flow and volume in humans. Neuroimage 24, 1–11.

Sabayan, B., Jansen, S., Oleksik, A.M., van Osch, M.J., van Buchem, M.A., van Vliet, P., de Craen, A.J., Westendorp, R.G., 2012. Cerebrovascular hemodynamics in alzheimer's disease and vascular dementia: a meta-analysis of transcranial doppler studies. Ageing Res. Rev. 11, 271–277.

Simon, M.J., Iliff, J.J., 2016. Regulation of cerebrospinal fluid (CSF) flow in neurodegenerative, neurovascular and neuroinflammatory disease. BBA 1862, 442–451.

Torre, J.C.D.L., 2004. Is alzheimer's disease a neurodegenerative or a vascular disorder? data, dogma, and dialectics. Lancet Neurol. 3, 184–190.

Tully, B., Ventikos, Y., 2009. Coupling poroelasticity and CFD for cerebrospinal fluid hydrodynamics. I.E.E.E. Trans. Biomed. Eng. 56, 1644–1651.

Tully, B., Ventikos, Y., 2011. Cerebral water transport using multiple-network poroelastic theory: application to normal pressure hydrocephalus. J. Fluid Mech. 667, 188–215.

Van, D.F., Wiesje, M., Skoog, I., Schneider, J.A., Pantoni, L., Mok, V., Chen, C.L.H., Scheltens, P., 2018. Vascular cognitive impairment. Nat. Rev. Dis. Primers 4, 18003.

Vardakis, J.C., Tully, B.J., Ventikos, Y., 2013. Multicompartmental poroelasticity as a platform for the integrative modeling of water transport in the brain. Computer Models in. Biomechanics.

Vardakis, J.C., Guo, L., Peach, T.W., Lassila, T., Mitolo, M., Chou, D., Taylor, Z.A., Varma, S., Venneri, A., Frangi, A.F., Ventikos, Y., 2019. Fluid–structure interaction for highly complex, statistically defined, biological media: Homogenisation and a 3D multi-compartmental poroelastic model for brain biomechanics. J. Fluids Struct. 91, 102641.

Yan, L., Liu, C.Y., Wong, K.P., Huang, S.C., Mack, W.J., Jann, K., Coppola, G., Ringman, J.M., Wang, D.J.J., 2018. Regional association of pCASL-MRI with FDG-PET and PiB-PET in people at risk for autosomal dominant alzheimer's disease. Neuroimage Clin 17, 751–760.

Zhang, N., Gordon, M.L., Goldberg, T.E., 2017. Cerebral blood flow measured by arterial spin labeling MRI at resting state in normal aging and alzheimer's disease. Neurosci. Biobehav. Rev. 72, 168–175.

Zhang, K., Herzog, H., Mauler, J., Filss, C., Okell, T.W., Kops, E.R., Tellmann, L., Fischer, T., Brocke, B., Sturm, W., 2014. Comparison of cerebral blood flow acquired by simultaneous [15O]water positron emission tomography and arterial spin labeling magnetic resonance imaging. J. Cereb. Blood Flow Metab. 34, 1373.

Zhang, Q., Stafford, R.B., Wang, Z., Arnold, S.E., Wolk, D.A., Detre, J.A., 2012. Microvascular perfusion based on arterial spin labeled perfusion MRI as a measure of vascular risk in alzheimer's disease. J. Alzheimers Dis. 32, 677–687.

Zimny, A., Sasiadek, M., Leszek, J., Czarnecka, A., Trypka, E., Kiejna, A., 2007. Does perfusion CT enable differentiating alzheimer's disease from vascular dementia and mixed dementia? A preliminary report. J. Neurol. Sci. 257, 114–120.